POLITECNICO DI MILANO
DEPARTMENT OF AEROSPACE ENGINEERING

POLITECNICO
MILANO 1863

SPACECRAFT ATTITUDE AND DYNAMICS

AA 2023-2024

Professor: Bernelli Zazzera Franco

Person Code	Surname	Name	Bachelor (type and University)
10717230	Beretta	Beatrice	Management Engineering - Politecnico di Milano
10726898	Juvara	Matteo Giovanni	Aerospace Engineering - Politecnico Di Milano
10782473	Miccoli	Francesco Antonio	Aerospace Engineering - Politecnico Di Milano
10973642	Separovic	Tomislav Marko	Mechanical Engineering - Instituto Tecnologico de Buenos Aires

Table 1: Team Members

July 29, 2024

Contents

List of Figures

List of Tables

Nomenclature

$\hat{S}$	Direction of the sun
ρ	Density of air
$\vec{B}$	Magnetic field
$\vec{F}$	Force acting on the spacecraft
$\vec{H}_r$	Inertia Wheel's Angular Momentum
C_D	Aerodynamic coefficient of drag
COM	Center of mass
$RAAN$	Right Ascension of the Ascending Node
x_B	x variable expressed in body frame
x_N	x variable expressed in inertial frame
$\dot{\vec{\omega}}$	Angular acceleration of the spacecraft
μ	Standard gravitational parameter of Earth
ϕ	First Euler Angle
ψ	Third Euler Angle
θ	Second Euler Angle
$\vec{M}$	Torque acting on the spacecraft
$\vec{r}$	Position of the spacecraft
$\vec{\omega}$	Angular velocity of the spacecraft
$A_{B/N}$	Rotation matrix from body frame to inertial frame
I	Inertia tensor

1 Introduction

The goal of designing and analyzing the attitude dynamics of a spacecraft, addressed in the following report, represents an excellent opportunity to gain a deeper understanding on how to analyze the more complex aspects of orientation control in space through the use of the MATLAB® Simulink environment.
In particular, the report focuses on modeling and determining the complete attitude dynamics and control loop of a mini-satellite. The objective of this mission is to detumble, point to a set location, and stabilize the satellite, complying with the constraints given.
The mission was completed satisfying some initial requirements, shown in the table below:

	Assigned Specifications	**Modifications**	**Motivation for Modifications**
Platform	Minisat (100-500 Kg)	None	/
Attitude Parameters	Euler Angles	None	/
Mandatory Sensors	Sun Sensors	Magnetometer, Gyroscope	For attitude determination
Actuators	3 Magnetic Coils 1 Inertia wheel	3 Reaction Wheels	See Sec. 2.6.2

The logical scheme of the simulation used to compute the results presented is shown in Fig. 1

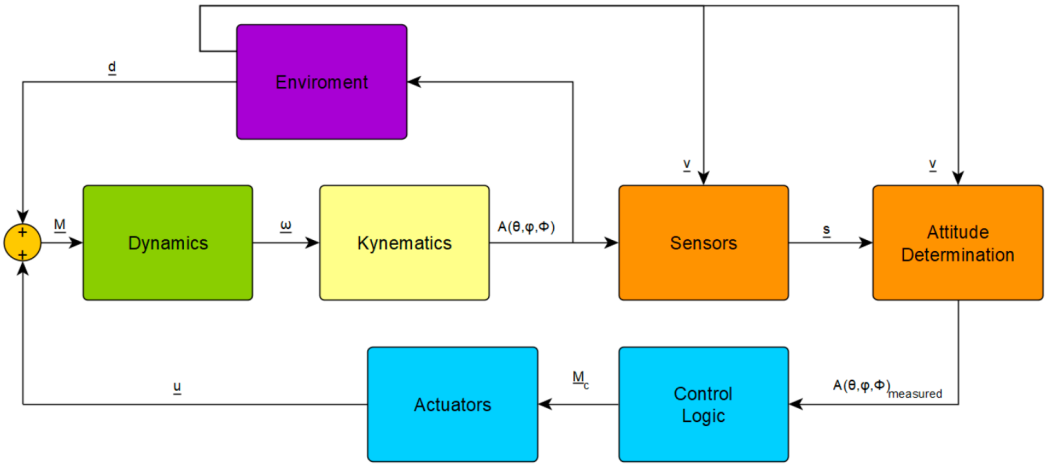

Fig. 1: Simulation block-diagram

1.1 Spacecraft Geometry

This report explores the analysis and control of a mini-satellite with dimensions of $60 \times 60 \times 80$ cm and a mass of 133.2 kg, basing the design on the existing satellite **DEMETER**[1], which has similar characteristics. The chosen geometry of the spacecraft is made up of a central rectangular body with a single solar panel positioned on the X-Z plane of the face facing upwards in the Z direction.

[1] `https://space.skyrocket.de/doc_sdat/demeter.htm`

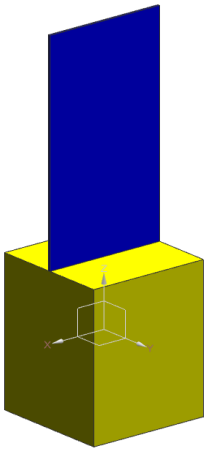

Fig. 2: mini-satellite design

The dimensions and the shape of the mini-satellite have been determined to best meet the specific mission requirements and to maximize the performance of the attitude control. This design also ensures the necessary space for accommodating the required sensors, actuators and subsystems.

1.2 Orbit Determination

A Sun Synchronous Orbit (SSO) has been selected, in particular a dawn dusk sun synchronous orbit, which means the satellite is always in sunlight to maximize the use of the solar sensors, one of mission's requirements. These sensors enable careful monitoring of the direction of the sun, providing the necessary information for the correct orientation of the satellite.
A SSO is a polar orbit with a slight precession of the Right Ascension of the Ascending Node (RAAN) of 1 degree eastward each day. This allows satellites on this orbit to pass over any given point on the Earth's surface at the same local mean solar time. In this report we neglected the precession of the orbit as it is minimal in the time-frame used.
The orbit is characterized by the parameters shown in the Table 2.

a	e	i	$RAAN$	ω	$Period$
6945 km	0	99.72°	57.84°	0°	5760 s

Table 2: Orbital parameters

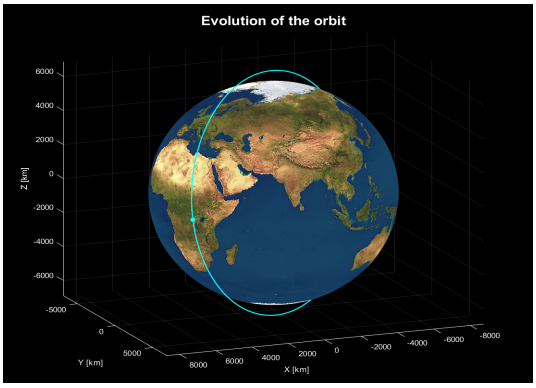

Fig. 3: Representation of the Orbit

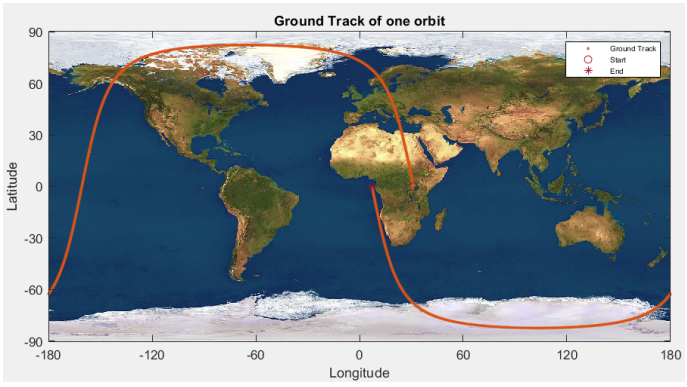

Fig. 4: Ground Track of the Orbit

2 Modeling

2.1 Dynamics

The rotation dynamics are described by Euler's rotation equation:

$$I\dot{\vec{\omega}} + \vec{\omega} \times \left(I\vec{\omega} + \vec{H}_r\right) = \vec{M}$$

where the term $\vec{M}$ can be expanded as:

$$\vec{M} = \vec{M}_d + \vec{M}_e \tag{1}$$

where $\vec{M}_d$ represents the torque produced by the disturbances and $\vec{M}_e$ is the control torque applied by the actuators and modeled as described in 2.6.

For the initial conditions it was decided to model the system as if the satellite deployment was not centered on the Center of Mass (COM) and as such it introduces an initial angular momentum h_0. Defining the deployment velocity v_0, the misalignment r_m and the mass of the satellite m and considering that the angular momentum is distributed equally between the three axes. Then $\vec{\omega}_0$ can be calculated as:

$$h_i = \frac{v_0\, r_m\, m}{\sqrt{3}} \qquad \vec{w}_0 = \left[\frac{h_i}{I_x}; \frac{h_i}{I_y}; \frac{h_i}{I_z}\right]$$

For this specific case, one obtains:

$$\vec{\omega}_0 = [0.3109;\ 0.3132;\ 0.5853] \quad \left[\frac{rad}{s}\right]$$

2.2 Kinematics

In order to follow the specifications of this project, Euler angles have been implemented for attitude determination. The components of the angular velocity vector can be written as a function of the three Euler angles and their first derivative. From these equations, the first time derivatives of the Euler angles can be obtained.

$$\begin{cases} \dot{\phi} = \frac{\omega_w cos(\psi) - \omega_u sin(\psi)}{cos(theta)} \\ \dot{\theta} = \omega_u cos(\psi) + \omega_w sin(\psi) \\ \dot{\psi} = \omega_v - (\omega_w cos(psi) - \omega_u sin(\psi)) \frac{sin(\theta)}{cos(\theta)} \end{cases} \tag{2}$$

These values are then integrated and converted to the $A_{B/N}$ matrix by using a 312 rotation matrix with the Euler angles implemented in the order seen above. The $A_{B/N}$ matrix is defined as follows:

$$\begin{bmatrix} cos\psi cos\phi - sin\psi sin\theta sin\phi & cos\psi sin\phi + sin\psi sin\theta cos\phi & -sin\psi cos\theta \\ -sin\phi cos\theta & cos\theta cos\phi & sin\theta \\ sin\psi cos\phi + cos\psi sin\theta sin\phi & sin\psi sin\phi - cos\psi sin\theta cos\phi & cos\psi cos\theta \end{bmatrix}$$

This set of equations alone is not sufficient to fully model the kinematics of a spacecraft, as in the equation for the first time derivative of ψ a singularity is present when θ tends to $(2n+1)\frac{\pi}{2}$. To solve this problem, a switch has to be implemented in the logic to change the problem to a 313 rotation matrix and its respective Euler equations, which have a singularity for θ tending to $n\pi$.

$$\begin{cases} \dot{\phi} = \frac{\omega_u sin(\psi) + \omega_v cos(\psi)}{sin(theta)} \\ \dot{\theta} = \omega_u cos(\psi) - \omega_v sin(\psi) \\ \dot{\psi} = \omega_w - (\omega_u sin(psi) + \omega_v cos(\psi) \frac{cos(\theta)}{sin(\theta)} \end{cases} \tag{3}$$

The switch acts when the cosine of θ falls below a certain threshold imposed prior. In order to avoid a continuous switch if the value of θ flutters around the threshold, an hysteresis system is put in place. This means that when the first switch takes place, the 313 equations keep being used until the sine of θ is greater than a second imposed threshold. Once this condition is not respected, the switch returns to its original configuration.

After a thorough simulation of the spacecraft's attitude, it was noticed that, in this particular case, the 312 Euler equations never reached a singularity, and a hysteresis system was not implemented to avoid unnecessary error factors due to the switch.

2.3 Disturbances

2.3.1 Gravity Gradient

The intensity of the gravity field depends on the distance from the center of the Earth. This means that each part of the spacecraft is affected by a slightly different gravity force. For spacecrafts that are not symmetric in the LVLH frame this causes a disturbance called gravity gradient. The moment generated by the gravity gradient can be expressed as:

$$\vec{M}_{GG} = (\vec{c} \times I\vec{c})\frac{3\mu}{r^3}$$

With $\vec{c}$ being the unitary vector that points from the spacecraft towards the earth, which can be calculated as:

$$\vec{c} = -A_{B/N}\frac{\vec{r}}{r}$$

2.3.2 Atmospheric Drag

The friction between the spacecraft and air particles in the atmosphere generates a disturbing torque, perturbing the dynamics of the satellite. The drag force acting on each panel of the spacecraft can be modeled as:

$$\vec{F_i} = \begin{cases} -\frac{1}{2}C_D\,\rho(h)\,\vec{v}_r\,(\vec{n}_i \cdot \vec{v}_r)\,A_i & \text{if} \quad \vec{n}_i \cdot \vec{v}_r > 0 \\ 0 \quad \text{if} \quad \vec{n}_i \cdot \vec{v}_r <= 0 \end{cases} \tag{4}$$

With $\vec{n}_i$ being the normal of each panel, A_i the area of each panel and $\vec{v}_r$ the velocity relative to earth's atmosphere in body frame:

$$\vec{v}_r = A_{B/N}\left(\vec{v} + \vec{r} \times \begin{bmatrix} 0 \\ 0 \\ \omega_\oplus \end{bmatrix}\right)$$

The altitude of the spacecraft is calculated taking into account the oblateness of the Earth and the air density is calculated using the Committee on Space Research (COSPAR) International Reference Atmosphere [2] with the formula:

$$\rho(h) = \rho_0 \exp(-\frac{h - h_0}{H})$$

The total torque is then given by:

$$M_{AD} = \sum \vec{r_i} \times \vec{F_i}$$

Where $\vec{r_i}$ is the distance from the center of the panel to the center of mass of the spacecraft.

The values of C_D, $\vec{n}_i$, A_i and $\vec{r_i}$ used can be found on Table 3

2.3.3 Solar Radiation Pressure

In a Low Earth Orbit (LEO) there are 3 main sources of radiation: direct sunlight, sunlight reflected from the Earth (also known as planetary albedo) and radiation from Earth. Out of this 3 direct sunlight is the most intense, although the earth albedo and radiation are not completely insignificant they present many difficulties to model them. For starters they can't be modeled as point sources of radiation because the Earth covers a significant percentage of the spacecraft's horizon. Also the albedo is highly dependent on the conditions on the surface, such as weather or if there is ground or water. Taking all this into account we decided to only model the effects of the sun radiation on the spacecraft and neglect the other radiation derived disturbances.

The solar radiation pressure is $P_s = F_c/c$ with F_c the intensity of the solar radiation and c the speed of light. For each panel of the spacecraft the force of the solar radiation can be modeled as:

$$\vec{F_i} = \begin{cases} -A_i\, P_s \left[(1-c_s)\,\hat{S} + 2\left(c_s\,\hat{S}\cdot\vec{n}_i + \frac{1}{3}c_d\right)\vec{n}_i\right]\hat{S}\cdot\vec{n}_i & if \quad \hat{S}\cdot\vec{n}_i > 0 \\ 0 \quad if \quad \hat{S}\cdot\vec{n}_i < 0 \end{cases}$$

With A_i being the area of each panel, c_s the specularity coefficient of the surface, c_d the diffusive coefficient of the surface, $\hat{S}$ the direction of the Sun in body frame and $\vec{n}_i$ the normal versor of each panel.

Then the total torque is given by:

$$M_{SRP} = \sum \vec{r}_i \times \vec{F}_i$$

Where $\vec{r}_i$ is the distance from the center of the panel to the center of mass.

It must be taken into account whether the Sun is being eclipsed by the Earth. This is done considering the Earth an oblong spheroid and calculating if the line that passes through the spacecraft and points towards the Sun intersects the Earth, in that case the sun is being eclipsed and $M_{SRP} = 0$.

The values of A_i, c_s, c_d, $\vec{n}_i$ and $\vec{r}_i$ used can be found on Table 4

2.3.4 Magnetic Disturbances

Due to its internal structure, the Earth generates a magnetic field. Its interaction with the electronic components on board generates a disturbing torque. The behavior of the Earth's magnetic field can usually be approximated to that of a dipole, but since the satellite is equipped with magnetic sensors and actuators and it is positioned in a LEO, a more detailed model is needed. For this reason, the magnetic field is calculated with the 13 order harmonic expansion of the International Geomagnetic Reference Field (IGRF) using the method detailed in [1]. The obtained magnetic field, in an inertial reference frame, can be rotated to the body frame with the formula:

$$\vec{B}_B = A_{B/N}\vec{B}_N$$

The magnetic disturbance torque can then be calculated as:

$$\vec{M}_{MAG} = \vec{m} \times \vec{B}_B$$

With $\vec{m}$ being the magnetic dipole moment. Considering the altitude at which the spacecraft orbits around Earth, it is expected for the magnetic disturbance to be dominant over all other disturbances, following NASA's guideline [3] we consider our satellite as Class I Spacecraft. With a specific magnetic dipole moment of $1 \times 10^{-3}\,\frac{A\,m^2}{kg}$.

After applying a security factor, the magnetic dipole moment assigned to the spacecraft is:

$$\vec{m} = [0.1332; 0.1332; 0.1332] A\,m^2$$

2.4 Sensors

2.4.1 Sun Sensor

The output of the digital sun sensor chosen is given as an elevation and rotation of the sun relative to its axis, and as such both its resolution and error are given as rotation and elevation angles. This means that to correctly model the sensor, the vector of the sun direction "$\hat{S_B}$" must first be converted to two angles: a rotation angle "α" and an elevation angle "h". These angles are sampled at the frequency of the sensor with a zero order hold, the error is then added through a random number generator and they're then quantized with the proper resolution. Using these two angles, the measured sun direction vector can be then reconstructed.

For this mission a Cubespace CubeSense Sun[2] was used.
The parameters of the chosen sun sensor are given in the Table 5.

Fig. 5: Cubespace cubesense sun

2.4.2 Magnetometer

In order to correctly model the magnetometer, the magnetic field is first sampled at the frequency of the sensor with a zero order hold, random noise is then added through a white noise band generator and in the end everything is quantized with the proper resolution.

For this mission a NewSpace NMRM-Bn25o485[3] was used.
The parameters of the chosen magnetometer are given in the Table 6.

Fig. 6: NewSpace MNRM Bn25o485

2.4.3 Gyroscope

To correctly model the output of the sensor, it is sufficient to add to the theoretical angular velocity the noise due to Angular Random Walk (ARW) and Rate Random Walk (RRW). First, the theoretical angular velocity has to be rotated from the body frame to the sensor frame, and then the ARW is added through a random number block with the right sampling time and variance. On the other hand, the RRW can be modeled through a random number block but has to be integrated through a time-discrete integrator using the sampling time of the sensor. Once the noise is added, the angular velocity is rotated back in the body

[2] https://satsearch.co/products/cubespace-gen2-cubesense-sun
[3] https://satsearch.co/products/newspace-systems-nmrm-bn25o485-magnetometer

frame.

For this mission, an Airbus' Astrix200 Fiber optic Gyroscope (FOG)[4] was used.
The parameters of the chosen gyroscope are given in the Table 7.

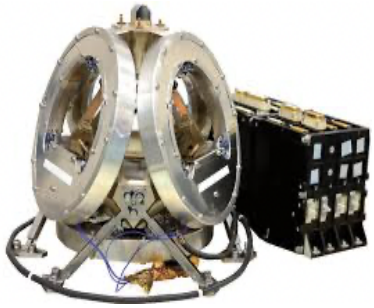

Fig. 7: Airbus' Astrix200 Fiber optic Gyroscope (FOG)

2.5 Attitude Determination

For attitude determination, a statistical method is used. The satellite obtains two measured vectors: $\vec{S}_B$ and $\vec{B}_B$, and knows the two inertial vectors $\vec{S}_N$ and $\vec{B}_N$. Due to the orbit of the satellite, the vectors $\vec{S}$ and $\vec{B}$ are almost perpendicular, which helps computing a successful attitude determination. The following B matrix can be constructed as:

$$B = \alpha_s \, \vec{S}_B \, \vec{S}_N^T + \alpha_b \, \vec{B}_B \, \vec{B}_N^T$$

The α values represent the precision of the measurements, with $\alpha_s + \alpha_b = 1$. These values are calculated to take into account the fact that the precision of the $\vec{B}$ vector depends on the magnitude of B.

$$P_s = \frac{1}{\theta/2 + \sigma_s} \quad P_b = \frac{B}{b/2 + \sqrt{N_b \, f}} \qquad \alpha_s = \frac{P_s}{P_s + P_b} \quad \alpha_b = \frac{P_b}{P_s + P_b}$$

Where θ is the angular resolution of the sun sensor in radians, σ_s is the standard deviation of the sun sensor in radians, B is the magnitude of the magnetic field, b is the resolution of the magnetic sensor, N_b is the noise power of the magnetic sensor and f is the sampling frequency of the magnetic sensor.

The matrix B can be decomposed using single-value decomposition as follows:

$$B = U \Sigma^T V^T$$

The direction cosine matrix can then be reconstructed as:

$$A_{B/N} = U \, diag[1, \, 1, \, det(U) \, det(V)] \, V^T$$

2.6 Actuators

2.6.1 Magnetic Coils

Magnetic actuators generate a torque through the interaction of the magnetic dipole induced in three coils and the Earth's magnetic field:

$$\vec{M}_e = \vec{m} \times \vec{B} \tag{5}$$

The model receives the magnetic dipole as an input from the control algorithm, controls its value to be within the values accepted by the chosen model, and outputs the computed torque to the dynamics subsystem.
The chosen magnetorquer is an MTQ800[5], this model can go up to $30 \, \mathrm{A \, m^2}$ and is considered to be installed in a 3-piece configuration parallel to the body axes.

[4] https://www.ixblue.com/wp-content/uploads/2021/12/datasheetastrix200.pdf
[5] https://satsearch.co/products/aac-clyde-mtq800-magnetorquers

2.6.2 Inertia and Reaction Wheels

A full set of reaction wheels has been chosen for the mission. This choice has been made based on different factors:

- The chosen orbit is polar; thus, the satellite experiences a substantial change in magnetic field strength and direction. This means that even if a single inertia wheel were installed, the craft could be unable to be controlled independently on three axis for the whole duration of the orbit.
- Reaction wheels are generally more accurate as they operate based on the conservation of angular momentum, allowing for precise control over rotational rates, which is particularly useful during inertial pointing;
- the reference satellite **DEMETER** uses a set of 4 reaction wheels.

The wheels model takes the desired control momentum as an input and solves a differential equation to compute the wheels torque $\dot{\vec{H}}_r$ and momentum $\vec{H}_r$:

$$\dot{\vec{H}}_r = -A^* \left(\vec{M}_C + \vec{\omega} \times A\vec{H}_r \right) \tag{6}$$

where A is a matrix with 3 rows and as many columns as the number of actuator, that depends on the mounting of the wheels with respect to the craft, and A^* is its pseudo-inverse.
After each step of the integration the computed effective torque M_e is found by inverting Eq. 6, the torque thus includes the term $\vec{\omega} \times A\vec{H}_r$ which is not considered in the left hand side of the dynamics equation.
The chosen model[6] can generate up to 1 N m s of momentum and 0.1 N m of torque.

3 Control

3.1 Introduction to the control problem and control logic

The control algorithm needs to be able to handle three different scenarios, which usually follow one another chronologically:

1. detumbling;
2. slew;
3. inertial pointing.

To be able to switch from one control law to another, a logic based on the measured angular velocity and pointing error is implemented, as shown in Fig. 8.
The switch from detumbling to slew is made when the angular velocity drops within a certain boundary set prior; to detect this event, the peaks of the signal are found by analyzing the first time derivative of the angular velocity. Whenever both a peak and a valley are within a set boundary, the control logic switches to slew.
Then, as the pointing error falls below a set tolerance, the control switches from a non-linear approach to a linear quadratic regulator.

3.2 Detumbling

The control law adopted for the detumbling of the satellite is based on the B-dot controller and therefore exploits the magnetorquers to perform all the required corrections.
This approach, whilst very simple, is very effective at high spin rates and leads to an angular rate that is sufficiently low to activate low refresh rate sensors and use them for a more precise control. The torque produced by a magnetorquer can be expressed as:

$$\vec{M}_C = \vec{m} \times \vec{B} \tag{7}$$

[6] `https://www.rocketlabusa.com/assets/Uploads/RL-RW-1.0-Data-Sheet.pdf`

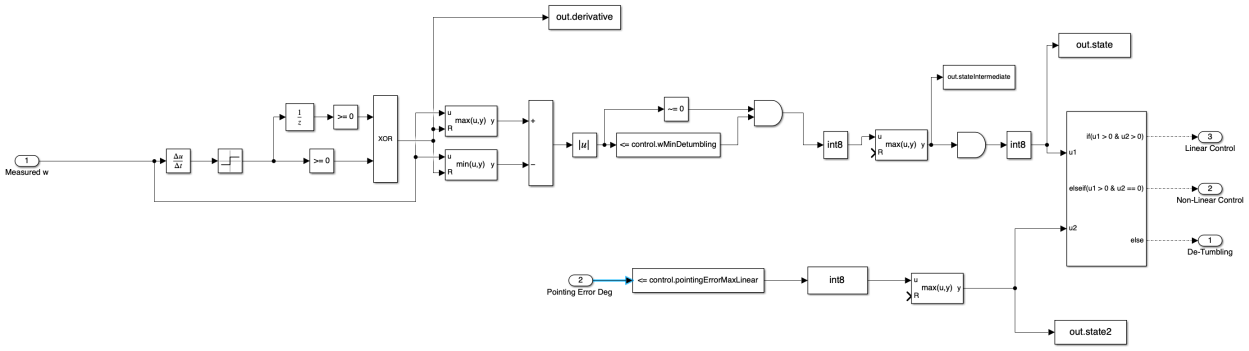

Fig. 8: Control choice subsystem

We can then take advantage of the magnetometer and gyroscope to compute the first time derivative of the magnetic field, which is essential in calculating the needed magnetic dipole:

$$\dot{\vec{B}} = -\left[\omega\times\right]\vec{B} \quad \Rightarrow \quad \vec{m} = -k_B\dot{\vec{B}} \tag{8}$$

in which the k_B gain is selected through a trial and error process.

3.3 Slew

Once the angular rate drops within a certain set boundary, the control is switched to slew. The control logic for this maneuver is based on a non-linear approach that tries to minimize both the pointing error and the angular velocity. In particular:

$$\vec{M}_C = -k_1\vec{\omega} - k_2\left(A_D^T - A\right)^V \tag{9}$$

where A_D is the target attitude and the k parameters are selected once again through a trial and error process.

3.4 Inertial pointing

The inertial pointing is based on a Linear Quadratic Regulator (LQR) which itself is based on the state space representation of the system.

3.4.1 State Space Representation

In order to correctly model a LQR, only the state space representation is needed:

$$\dot{\vec{x}} = \underline{\underline{A}}\cdot\vec{x} + \underline{\underline{B}}\cdot\vec{u} \tag{10}$$

where the state $\vec{x}$ is defined as:

$$\vec{x} = [\omega_x,\ \omega_y,\ \omega_z,\ q_0,\ q_1,\ q_3,\ q_4] \tag{11}$$

The system is then linearized around the target state for earth pointing:

$$\vec{x}_d = [0,\ n,\ 0,\ \bar{q}_1,\ \bar{q}_2,\ \bar{q}_3,\ \bar{q}_4] \tag{12}$$

where the quaternion follows the scalar first norm. This results in the following equation:

$$A = \begin{bmatrix} 0 & 0 & \frac{I_Z-I_Y}{I_X}n - H_Y^W & 0 & 0 & 0 & 0 \\ 0 & 0 & 0 & 0 & 0 & 0 & 0 \\ \frac{I_Y-I_X}{I_Z}n + H_Y^W & 0 & 0 & 0 & 0 & 0 & 0 \\ \frac{1}{2}\bar{q}_4 & -\frac{1}{2}\bar{q}_3 & \frac{1}{2}\bar{q}_2 & 0 & 0 & 0 & 0 \\ \frac{1}{2}\bar{q}_3 & \frac{1}{2}\bar{q}_4 & -\frac{1}{2}\bar{q}_1 & 0 & 0 & 0 & 0 \\ -\frac{1}{2}\bar{q}_2 & \frac{1}{2}\bar{q}_1 & \frac{1}{2}\bar{q}_4 & 0 & 0 & 0 & 0 \\ -\frac{1}{2}\bar{q}_1 & -\frac{1}{2}\bar{q}_2 & -\frac{1}{2}\bar{q}_3 & 0 & 0 & 0 & 0 \end{bmatrix} \quad B = \begin{bmatrix} \frac{1}{I_X} & 0 & 0 \\ 0 & \frac{1}{I_Y} & 0 \\ 0 & 0 & \frac{1}{I_Z} \\ 0 & 0 & 0 \\ 0 & 0 & 0 \\ 0 & 0 & 0 \\ 0 & 0 & 0 \end{bmatrix} \tag{13}$$

3.4.2 Linear Quadratic Regulator

The next step in the design of the LQR is the definition of the cost function; a standard quadratic function is sufficient for this application:

$$J = \frac{1}{2}\int_0^{t_f} \left(\vec{u}^R Q \vec{u} + \vec{u}^T R \vec{R}\right) dt \tag{14}$$

For this equation to be complete, the weight matrices Q and R need to be defined. There are different approaches to this problem. A first guess of the diagonal values was chosen, keeping in mind that larger values on the diagonal elements of the weight matrices result in a bigger penalization of the deviations in those state variables inside the cost function.
After that, a trial and error process led to the final product used for the simulation:

$$Q = diag\left([100,\ 100,\ 100,\ 1e-4,\ 1e-4,\ 1e-4,\ 1e-4]\right) \tag{15}$$

$$R = diag\left([1,\ 1,\ 1]\right) \tag{16}$$

Then, by means of Matlab's *lqr* function, the associated Riccati equation is solved and an optimal state feedback matrix K is computed:

$$K = lqr\left(A,\ B,\ Q,\ R\right); \tag{17}$$

This matrix is then used to compute the desired control momentum:

$$\vec{u} = K\left(\vec{x}_d - \vec{x}\right) \tag{18}$$

4 Results

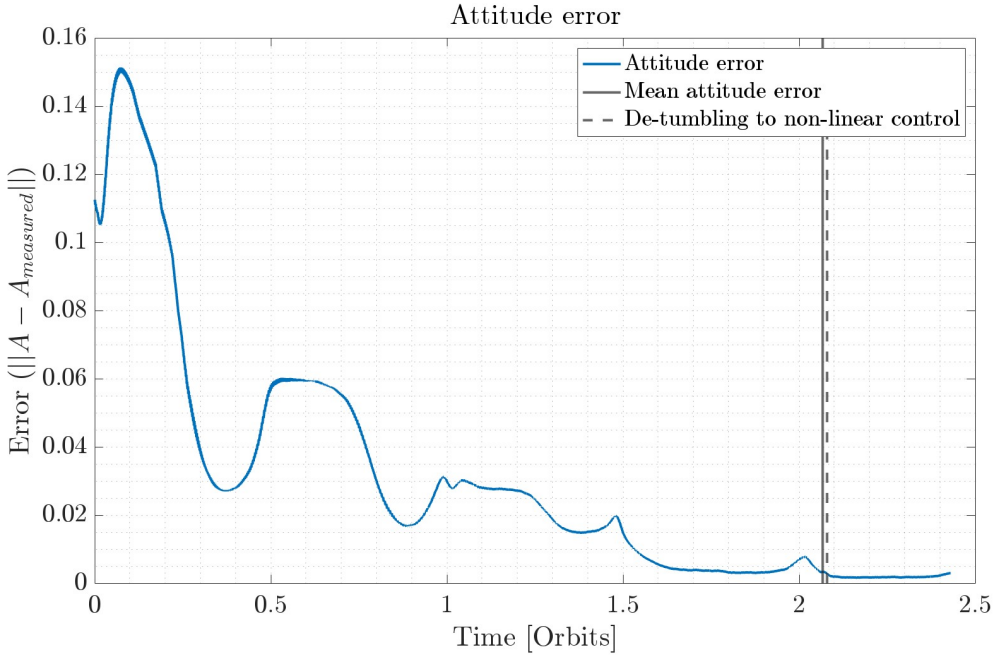

Fig. 9: Attitude error

In the Figure 9 the error of the attitude determination is presented. It is notable that this error is most significant during the tumbling phase, as the sensors don't have a fast enough sample rate to maintain a good attitude determination.

4.1 De-tumbling

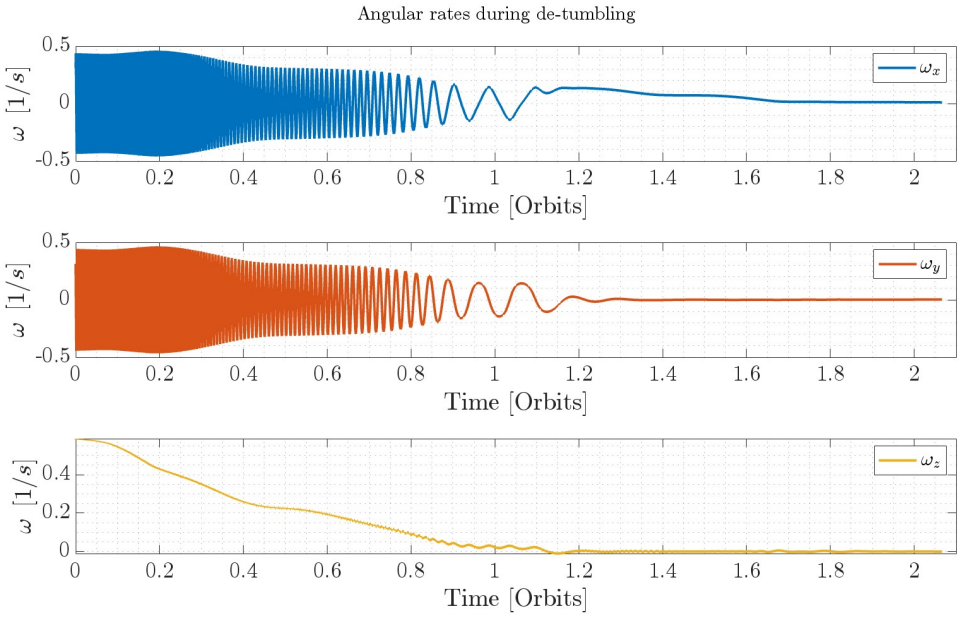

Fig. 10: Angular rates during de-tumbling

In Figure 10 the angular rates of the spacecraft during de-tumbling are presented. This angular rates have a tendency to decrease and in particular ω_x and ω_y oscillate, this correspond to the maximum and intermediate inertia directions, although they have almost the same inertia. While ω_z does not oscillate and corresponds to the minimum inertia direction. In Figure 11 the total angular momentum is plotted and it's noticeable how it continuously goes down during de-tumbling.

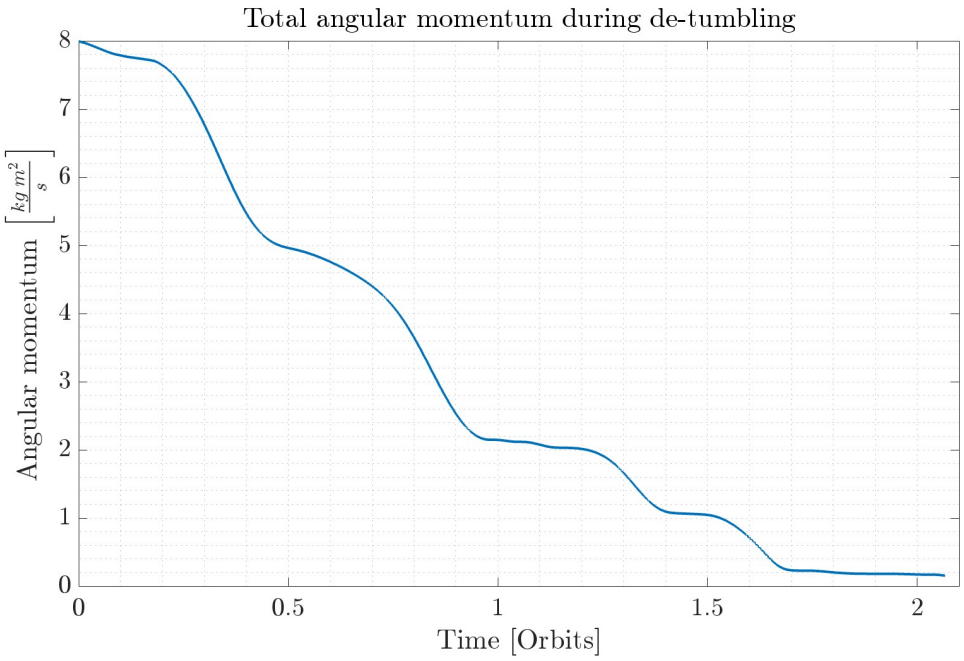

Fig. 11: Total angular momentum during de-tumbling

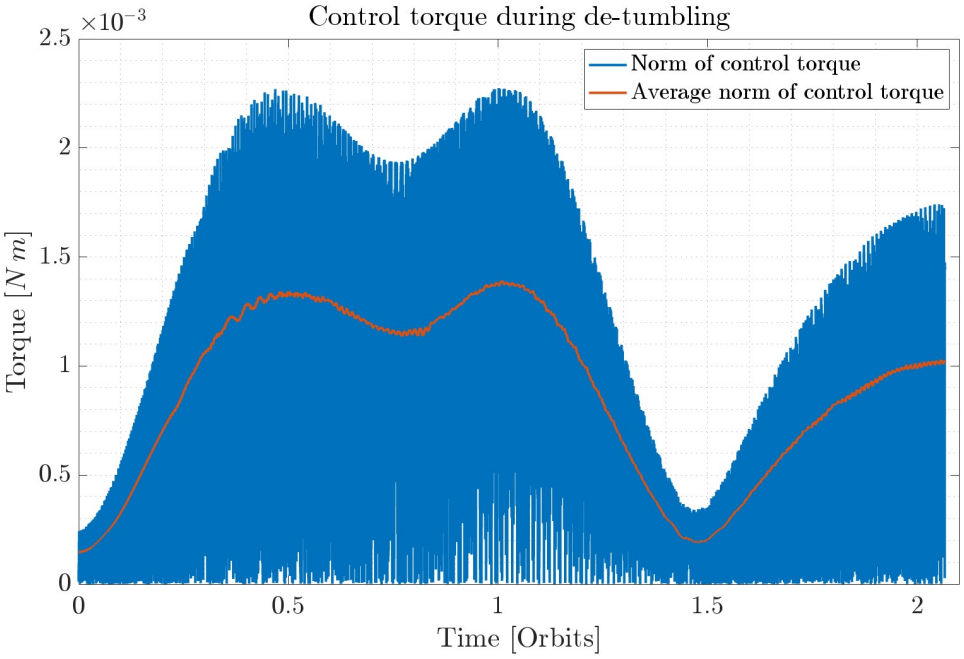

Fig. 12: Control torque during de-tumbling

In the Figure 12 the control torque during de-tumbling is presented. A limiting factor is that by using magnetic coils the control torque must be perpendicular to the direction of the magnetic field. Which means that the direction of the possible control torque depends on the position of the spacecraft on it's orbit, this causes that the spacecraft must wait until it's in the right position to apply the control torque.

4.2 Pointing error during slew maneuver and earth pointing

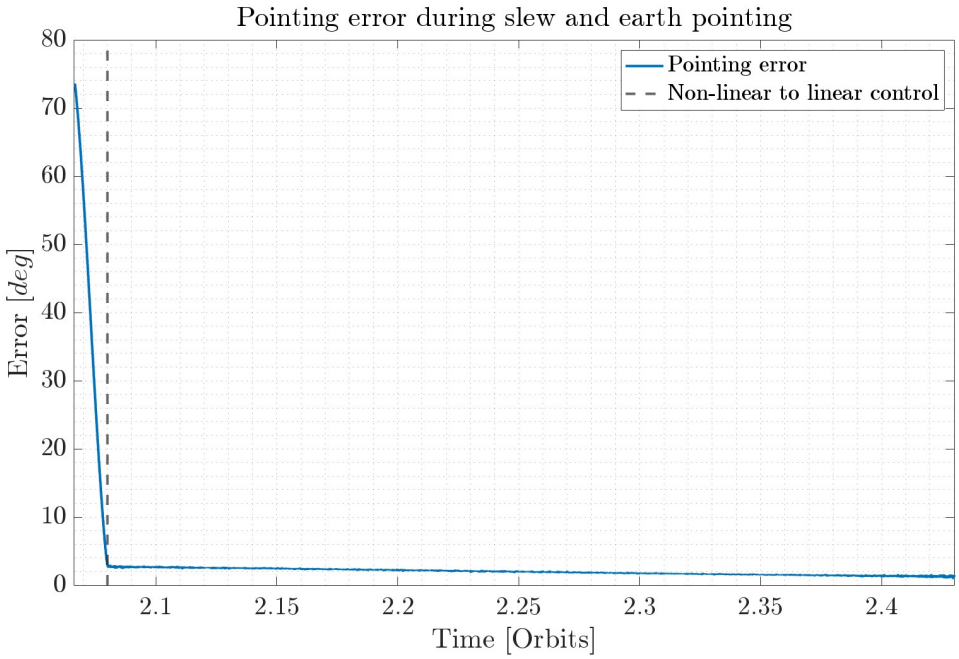

Fig. 13: Caption

In the Figure 13 the pointing error of the spacecraft is plotted. After the de-tumbling maneuver the pointing error is significant, it is quickly decreased with non-linear control which then switches to linear control to increase the precision.

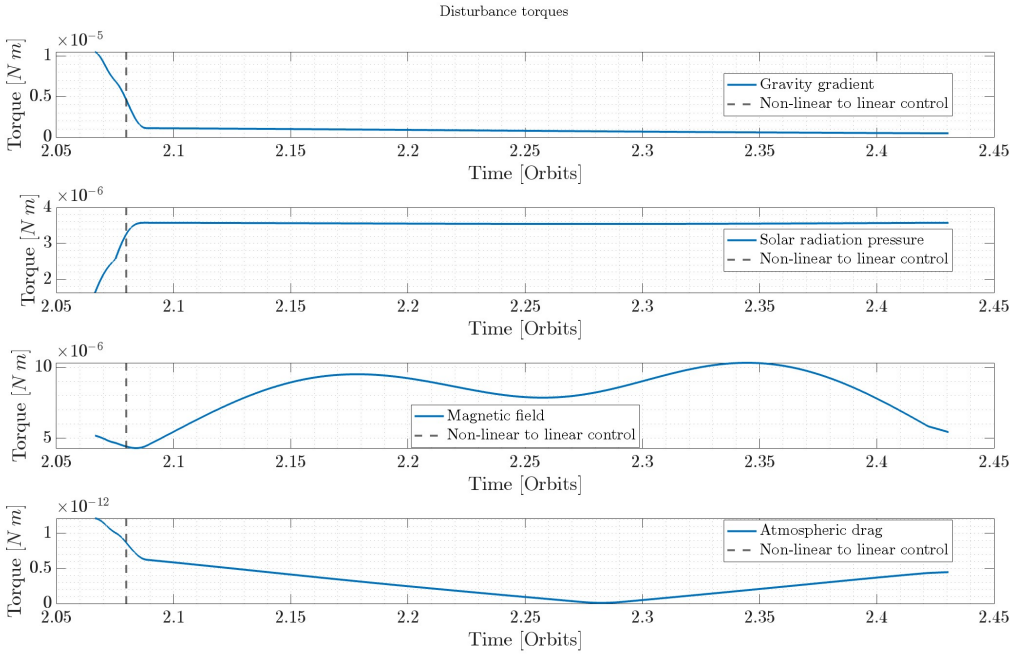

Fig. 14: Disturbance torques

In Figure 14 the norms of the disturbance torques are plotted.

It is notable how the gravity gradient torque follows a similar shape to the pointing error, as it tends to zero when the pointing error is zero.

The solar radiation pressure torque remains constant once the satellite is pointing correctly as the solar panel is pointed towards the sun.

As expected the magnetic torque is the most significant and oscillates due to the changes of the magnetic field between the poles and the equator.

The atmospheric drag torque depends highly on the rotation of the satellite on the z axis, as the solar panel is nominally perpendicular to the air flow but any error in the rotation exposes it to the flow and generates air drag.

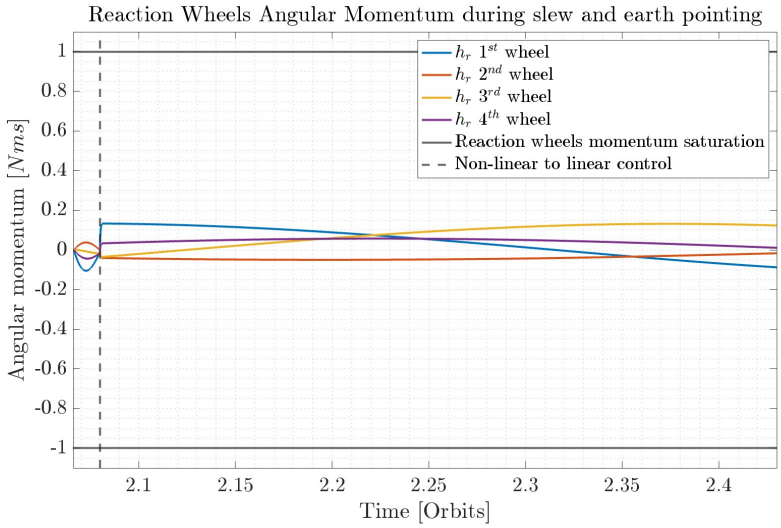

Fig. 15: Reaction wheels angular momentum during slew and earth pointing

In Figure 15 the angular momentum of the reaction wheels is plotted. The reaction wheels are mostly used

to compensate the disturbance torques.

5 Conclusion

Since the spacecraft used in this mission is intrinsically unstable due to its geometry and the type of orbit used, the use of active control is imperative to achieve the satellite's main goal and has proved to be capable of compensating the spacecraft's instability.
It has been proven possible to do attitude determination with just a sun sensor and magnetometer, although this is only possible in some specific orbits and can cause some error in moments when angle between the direction of the sun and the magnetic field is small.
It has been proven possible to de-tumble the satellite using only magnetic coils, this comes at the cost of having to wait to be at specific points on the orbit to be able to generate the required control torques.
The reaction wheels have proven to be capable to compensate all disturbance torques and when needed they can be desaturated using the magnetic coils.
In future missions the magnetic coils and inertia wheels can be used at the same time to maximize the control of the spacecraft.

6 Appendix

6.1 Tables

Panel	C_D	$\vec{n}_i$	A_i $[m^2]$	$\vec{r}_i$ $[cm]$
Face +x	2	$[1;0;0]$	0.48	$[30;0;0]$
Face +y	2	$[0;1;0]$	0.48	$[0;30;0]$
Face -x	2	$[-1;0;0]$	0.48	$[-30;0;0]$
Face -y	2	$[0;-1;0]$	0.48	$[0;-30;0]$
Face +z	2	$[0;0;1]$	0.36	$[0;0;37.2973]$
Face -z	2	$[0;0;-1]$	0.36	$[0;0;-42.7027]$
Solar Panel +y	2	$[0;1;0]$	0.72	$[0;0;97.2973]$
Solar Panel -y	2	$[0;-1;0]$	0.72	$[0;0;97.2973]$

Table 3: Data for Air Drag

Panel	c_s	c_d	$\vec{n}_i$	A_i $[m^2]$	$\vec{r}_i$ $[cm]$
Face +x	0.5	0.1	$[1;0;0]$	0.48	$[30;0;0]$
Face +y	0.5	0.1	$[0;1;0]$	0.48	$[0;30;0]$
Face -x	0.5	0.1	$[-1;0;0]$	0.48	$[-30;0;0]$
Face -y	0.5	0.1	$[0;-1;0]$	0.48	$[0;-30;0]$
Face +z	0.5	0.1	$[0;0;1]$	0.36	$[0;0;37.2973]$
Face -z	0.5	0.1	$[0;0;-1]$	0.36	$[0;0;-42.7027]$
Solar Panel +y	0.1	0.1	$[0;1;0]$	0.72	$[0;0;97.2973]$
Solar Panel -y	0.1	0.1	$[0;-1;0]$	0.72	$[0;0;97.2973]$

Table 4: Data for Solar Radiation Pressure

Resolution	0.2°
Sigma	0.1°
Detection FOV	166°
Update rate	2 Hz

Table 5: Sun Sensor parameters

Measurement range	± 60000 nT
Resolution	8 nT
Update rate	$<$ 18 Hz
Noise power	16 $\frac{nT^2}{Hz}$

Table 6: Magnetometer parameters

Sampling Frequency	100 Hz
Angle Random Walk*	0.0001 $^\circ/\sqrt{h}$
Bias Stability	0.0005 $^\circ/h$

Table 7: Gyroscope parameters

* The Angle Random Walk is valid at the beginning of the life cycle of the sensor (BoL).

References

[1] Jeremy Davis. Mathematical modeling of earth's magnetic field. Technical report, Virginia Tech, 2004.

[2] COSPAR Working Group IV. Cospar international reference atmosphere. *Akademie-Verlag*, 1972.

[3] S. Schalkowsky and M Harris. Spacecraft magnetic torques. Technical report, National Aeronautics and Space Administration, 1969.